



Original software publication

# MATBOX: An Open-source Microstructure Analysis Toolbox for microstructure generation, segmentation, characterization, visualization, correlation, and meshing



F.L.E. Usseglio-Viretta<sup>a,\*</sup>, P. Patel<sup>a</sup>, E. Bernhardt<sup>a</sup>, A. Mistry<sup>b</sup>, P.P. Mukherjee<sup>c</sup>, J. Allen<sup>d</sup>, S.J. Cooper<sup>e</sup>, J. Laurencin<sup>f</sup>, K. Smith<sup>a</sup>

<sup>a</sup> Center for Energy Conversion & Storage Systems, National Renewable Energy Laboratory, Golden, CO, 80401, USA

<sup>b</sup> Chemical Sciences & Engineering Division, Argonne National Laboratory, Lemont, IL 60439, USA

<sup>c</sup> School of Mechanical Engineering, Purdue University, West Lafayette, IN 47907, USA

<sup>d</sup> Computational Science Center, National Renewable Energy Laboratory, Golden, CO 80401, USA

<sup>e</sup> Dyson School of Design Engineering, Imperial College London, London, SW7 2DB, UK

<sup>f</sup> CEA-LITEN, 17 rue des martyrs, F-30854 Grenoble, France

## ARTICLE INFO

### Article history:

Received 18 May 2021

Received in revised form 9 August 2021

Accepted 19 November 2021

### Keywords:

Microstructure generation  
Microstructure segmentation  
Microstructure characterization  
Microstructure meshing

## ABSTRACT

MATBOX is an easy-to-use, all-in-one, MATLAB application for microstructure numerical analysis, including microstructure numerical generation, image filtering and microstructure segmentation, microstructure characterization, three-dimensional visualization, microstructure parameters correlation, and microstructure meshing. MATBOX was originally developed to analyse electrode microstructures for lithium-ion batteries; however, the algorithms provided by the toolbox are widely applicable to other heterogeneous materials. The toolbox provides a user-friendly experience thanks to a Graphic-User Interface.

© 2021 Published by Elsevier B.V. This is an open access article under the CC BY license (<http://creativecommons.org/licenses/by/4.0/>).

## Code metadata

Current code version	V1.0
Permanent link to code/repository used of this code version	<a href="https://github.com/ElsevierSoftwareX/SOFTX-D-21-00097">https://github.com/ElsevierSoftwareX/SOFTX-D-21-00097</a>
Code Ocean compute capsule	
Legal Code Licence	BSD
Code versioning system used	git
Software code languages, tools, and services used	MATLAB 2019+
Compilation requirements, operating environments & dependencies	MATLAB 2019+ with 'Image Processing Toolbox'
If available Link to developer documentation/manual	<a href="https://github.com/NREL/MATBOX_Microstructure_analysis_toolbox/tree/master/Documentation">https://github.com/NREL/MATBOX_Microstructure_analysis_toolbox/tree/master/Documentation</a>
Support email for questions	<a href="mailto:Francois.UsseglioViretta@nrel.gov">Francois.UsseglioViretta@nrel.gov</a>

## 1. Motivation and significance

Lithium-ion battery (LIB) electrodes performances are strongly correlated with their microstructure [1–3]. Most macroscale electrochemical battery models use the pseudo-2D formulation originally proposed by Newman and coworkers [4], that abstracts

the heterogeneous electrode materials with a set of microstructure parameters (e.g., particle size). These parameters are typically extracted from the analysis of 3D microstructure volume data obtained with Focused Ion Beam Scanning Electron Microscopy (FIB-SEM) or X-ray computed tomography (CT) [5,6]. The raw data obtained from these 3D imaging experiments is a 3D array for which each pixel (voxel in 3D) has a brightness value, that reflects the local sensitivity of the medium in regards with the imaging experiments. While analysis can be done at this stage, it is not the desired state as voxels do not identify each phase precisely. There is instead a distribution of

\* Corresponding author.

E-mail addresses: [Francois.UsseglioViretta@nrel.gov](mailto:Francois.UsseglioViretta@nrel.gov) (F.L.E. Usseglio-Viretta), [jerome.laurencin@cea.fr](mailto:jerome.laurencin@cea.fr) (J. Laurencin).

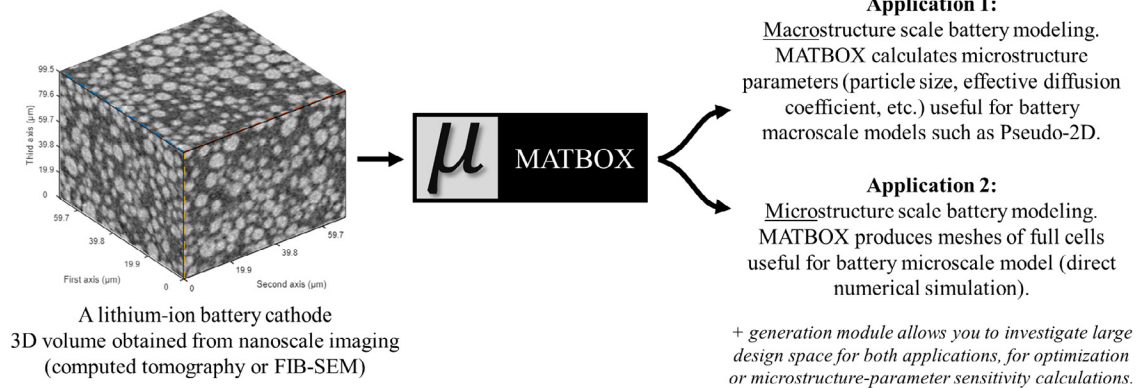


Fig. 1. Main applications of MATBOX.

grey level value (usually represented through a histogram). Volumes are then ‘segmented’ or ‘binarized’ so that each voxel is assigned to a given phase, typically the pore or void domain, and the solid phase(s). Once segmented, the electrode microstructure is characterized (i.e., microstructure parameters relevant to the application are calculated). While suitable for design guidance and being fairly successive to match experimental data [2,7], these models are intrinsically restricted by their macroscale approach and microstructure simplification [8]. To remedy these limitations, microscale models [8–14] are explicitly solving the system of equations directly on the microstructure geometry, removing both microstructure assumptions and parameters. Microscale models are especially relevant to investigate impact of microstructure heterogeneities and local features (e.g., cracks) otherwise neglected by their macroscale counterpart on electrochemical performances, although at the price of a much higher CPU and RAM cost.

Both modelling approaches require time-consuming pre-processing steps: segmentation and microstructure characterization for macroscale models, and segmentation and microstructure meshing for microscale models. MATBOX provides numerical algorithms embedded in a user-friendly graphical user interface (GUI) to streamline the whole process. Furthermore, to enable wide design space analysis and complement imaging capabilities, microstructure generation algorithms are also included (both active material and additive phases) in the toolbox. This toolbox has been used for characterizing LIB electrode microstructures in previous works [1,15,16], and for providing full cell meshes for microscale electrochemical LIB model [8]. Fig. 1 illustrates the main applications of MATBOX.

In addition to in-house algorithms, MATBOX uses third-party open-source software: Taufactor [17] from Dr. Samuel Cooper and Iso2mesh [18] from Dr. Qianqian Fang, respectively for tortuosity factor calculations and microstructure meshing. In addition, the toolbox uses third-party algorithms: xlscol [19], DataHash [20], Noiselevel [21], and Screenshot [22], respectively used to help exporting data in excel files, compare microstructure states in iterative algorithms through their hash value, estimate image noise level before and after image filtering, and copy figure from MATLAB App design. Algorithm from Dr. Aashutosh N. Mistry [23] is also used for one of the methods employed in the microstructure generation module, for additive phase generation. Thanks to its modular and open-source approach, MATBOX can integrate subsequent third-party algorithms from the LIB community, eventually building a reference in the field that would dramatically help improving result reproducibility and promoting open-source algorithms distribution.

MATBOX installation is explained in the documentation. The user can either package the app in MATLAB or directly run the file

Main\_menu.mlapp located in \MATBOX\_Microstructure\_analysis\_toolbox\src\Main\_menu\from MATLAB App designer. MATBOX welcomes the user with a main menu from which various modules can be called (cf. Fig. 2). Each module has its own GUI with a detailed documentation available in \MATBOX\_Microstructure\_analysis\_toolbox\Documentation\.

## 2. Software description

### 2.1. Software architecture

MATBOX is divided into several modules, one for each microstructure-related activity. Toolbox modules are connected through their inputs/outputs, as described in Fig. 3. The characterization module occupies a central place as it can take inputs from the generation module and the filtering and segmentation module, while its outputs are used for the properties correlation module and the microstructure and results visualization module.

### 2.2. Software functionalities

Module functionalities are introduced below and illustrated in Fig. 4. Detailed explanations of each module can be found in the toolbox documentation, with only a summary provided below. Methods and algorithms are detailed in the documentation and in the various references listed below.

- **Microstructure generation module**  
Three-dimensional microstructure imaging requires expensive equipment, time, and skilled workers that limit availability and quantity of data. Furthermore, the microstructure design space is restricted by existing electrode materials, preventing upstream microstructure scale modelling. Microstructure generation algorithms allow to numerically generate 3D microstructures that can be used for design space analysis otherwise not possible. It is valuable to evaluate ‘what if’ microstructures that can later motivate manufacturers to experimentally test promising architectures. Experimental imaging has intrinsic limitations that may result in not being able to distinguish one or several phases of the medium. For instance, X-ray computed tomography of lithium-ion battery electrodes such as NMC and graphite does not resolve the additive phases (carbon-black, for improved electron conductivity and binder, for mechanical integrity), that are then not distinguishable from the pore domain [1]. Such additives have practical impact, as they modify the effective electrolyte diffusion coefficient and the electrochemically active interfacial area between the active material and the electrolyte [1,23,24]. Microstructure

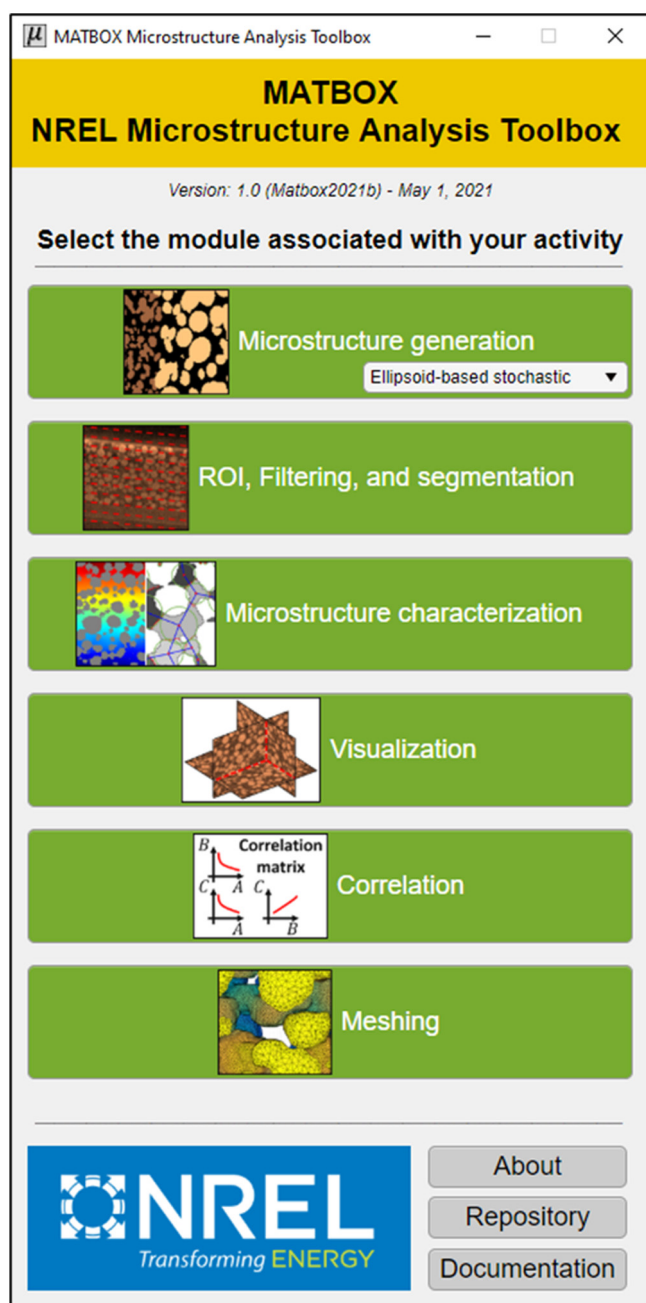


Fig. 2. Microstructure analysis toolbox main menu. Each module has its own GUI.

generation module includes both active material generation and additives generation.

Active material generation submodule uses an in-house stochastic,  $n$ -phase, ellipsoid-based, microstructure algorithm with fine control of volume fractions, particle size, elongation, and orientation distributions all along the electrode thickness allowing generating graded materials. Particle overlapping is user-controlled independently for each phase  $i$  - phase  $j$  permutation which allows to reach high density microstructures, effectively avoiding packing density limit (maximum packing density for randomly distributed non-overlapping ideal spheres is 63.4% [25]). Furthermore, particle generation order can be tuned to avoid the algorithm to stall for some microstructures that could be challenging to generate without it (for instance, generating

larger particles first then smaller particles has higher chance of success compared with the reverse order or even without any order – see documentation for further explanation).

Additive phase generation submodule provides two algorithms the user can choose between. First is an in-house deterministic algorithm for which additive phase is generated preferentially between particles non far from each other, so that it will create bridges between particles. The algorithm produces similar output as the “binder bridge” level-set approach proposed by Trembacki et al. [26,27], although with a different method. In this work, the pore size  $c$ -PSD( $x$ ) is first calculated using a spherical approach (continuous particle size method [28]). The original algorithm then iterates over a distance  $d$ , marking pore voxels for which  $c$ -PSD( $x$ ) <  $d$ . If the as-marked voxels are not enough to reach the additive target volume fraction, then all of them are assigned to the additive phase and then  $d$  is incremented until the additive volume fraction is reached. If too many voxels have been identified, only a subset of them are assigned to the additive phase to match its target volume fraction. A second algorithm developed by A. Mistry, K. Smith and P.P. Mukherjee [23] uses an energetic approach, where candidate voxels (candidate voxels have at least one solid neighbour and are within the background phase) assignment to the additive phase is based on an energy towards deposition on the pre-existing active material network or on the pre-deposited new additive phase. A user-defined morphology parameter  $\omega$  (adimensional, [0,1]) is used to bias the energy towards deposition for the candidate voxel, preferentially on existing active material ( $\omega = 0$ ) or on pre-deposited additive phase ( $\omega = 1$ ) resulting in different additive morphologies. The second method has been indirectly validated in a previous work as it provides geometries with tortuosity factor matching experimental data [1].

- Region of interest (ROI) selection, filtering, and segmentation module

This module provides the user with a variety of image processing tasks. Region of interest selection (including rotation), upscaling and downscaling for both grey-level and segmented volumes, grey-level in-depth analysis (especially to spot, if any, deviations along axis that would determine how to perform segmentation), contrast correction (e.g., histogram equalization), image filtering (anisotropic diffusion filter [29] and non-local mean filter [30]), and segmentation (local and global thresholding [31]). While methods currently available in this module are quite simple, they nevertheless appear sufficient to segment NMC and graphite electrode volumes from the NREL microstructure library [32] using a combination of image filtering, contrast correction and threshold-based segmentation. Instead, the module focuses on delivering a user-friendly experience to improve productivity. Furthermore, each action is logged into a csv file (i.e., a history log) that can be valuable to help implementing a systematic segmentation approach on large set of volumes to ensure segmentation coherence between all samples.

In addition to the above-mentioned image processing tasks, a segmentation sensitivity analysis can be performed to quantify the microstructure parameter errors induced by an uncertainty on the segmentation threshold. This is especially valuable for blind-segmentation, for which the user does not know the actual volume fractions (and therefore cannot use this information for guidance) and hesitates between an upper and a lower threshold that both look visually correct. This is particularly valuable for error propagation analysis, from microstructure segmentation error to macro-scale electrochemical model prediction errors.

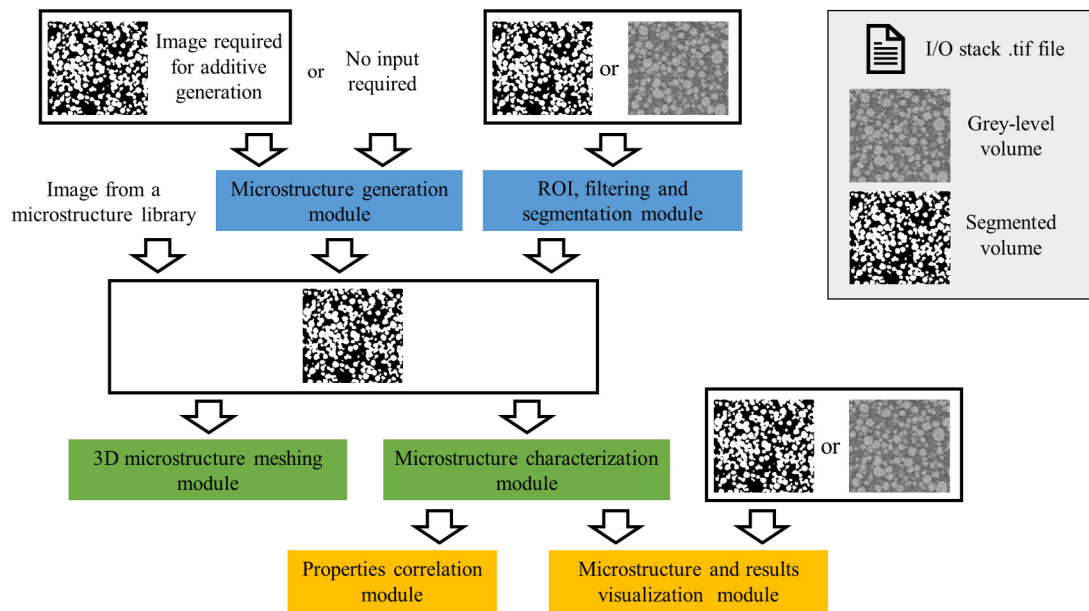


Fig. 3. Microstructure analysis toolbox module inputs/outputs connectivity.

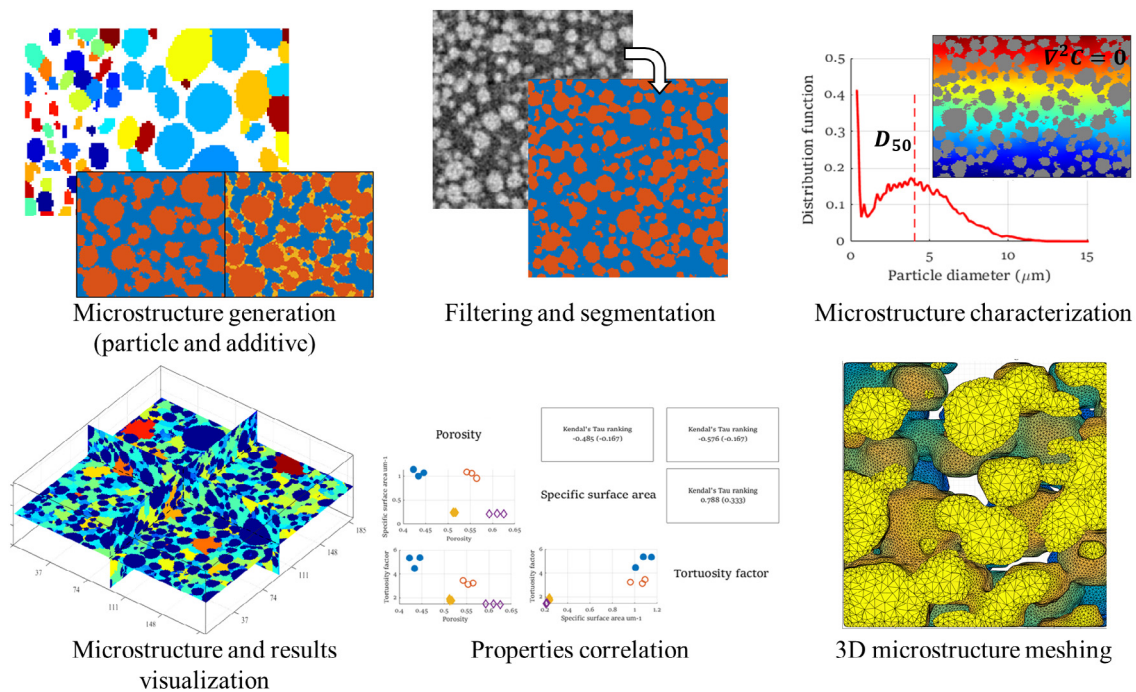


Fig. 4. Illustration of the Microstructure analysis toolbox modules.

- **Microstructure characterization and homogenization module**  
The module provides calculations of various metrics useful for LIB modelling: volume fractions, connectivity (both isotropic and directional), tortuosity factor (using TauFactor [17]), geometric tortuosity, specific surface area, particle size, particle identification and morphology. Parameter definitions and methods are explained in previous works [1, 15,16]. A special attention is dedicated for particle analysis with several in-house algorithms available (including discrete particle size algorithms for particle identification and morphology analysis), as particle size quantification within connected networks is highly dependent with the numerical method [16,28].

Module offers automated voxel size dependence analysis, through iterative downscaling (to evaluate microstructure parameter error induced by limited image resolution) and automated representative volume element (RVE) analysis [15,33] (to evaluate microstructure parameter error induced by limited field of view), as well as batch calculations to characterize multiple volumes in a row. RVE size is parameter-dependent [15], as well as voxel size dependence [1,16], therefore the user can select which microstructure parameters to perform these analyses. In addition, the user can finely adapt the RVE analysis, by choosing between two main approaches. First method consists in cutting the microstructure volume into independent (i.e., non-overlapping) subvolumes of the same size and with a user-specified

aspect ratio, and to calculate microstructure properties for each of these subvolumes. The relative standard deviation is then calculated considering all the results. The process is repeated with varying subvolume size to produce the curve relative standard deviation as a function of subvolume size. When the curve crosses a user-defined relative standard deviation threshold, then the representative volume element size of this sample (but not necessary of the material as a whole) is found. Volumes larger than the as-obtained threshold volume are considered to be representative of the electrode volume, thus their microstructure parameters can be used with confidence in macroscale models. A more refined explanation of RVE is provided in the toolbox documentation. A RVE analysis requires hundreds of calculations per volume and per microstructure property. This task is completely automated in the toolbox, saving manpower. The second method consists in growing a unique subvolume either from the field of view centroid or from one of its extremity and calculating the microstructure parameters for each subvolume size until convergence. This second approach is mainly included for the sake of completeness as the first method is recommended as thoroughly explained in the toolbox documentation.

- **Microstructure and results visualization.**  
Other modules generate 2D graphs to illustrate results. However, 3D visualization may be more relevant on some occasions. This module produces 3D visualizations of the microstructure itself and of microstructure parameters defined voxel-wise (e.g., particle size). Note that to visualize such microstructure parameters the user needs to run the characterization module to produce results first. The module also provides side-by-side comparison of gray level and segmented volumes, to visually evaluate the relevance of the segmentation, with overlay and checkerboard visualizations available to help the comparison.
- **Properties correlation.**  
Establishing correlations between microstructure properties provides a better understanding of their intrinsic relationships, help identifying independent parameters, and allow predicting microstructure properties. The most classic example would be the tortuosity factor as a function of porosity. This module allows you to load selected results from multiple microstructure characterization calculations quickly to produce correlation matrix-type figures. This module is especially valuable if your database contains dozens of microstructures and can reveal unsuspected correlations.
- **Meshing.**  
The module enables you to create volumetric tetrahedron-based meshes from a single n-phase volume (e.g., meshing a unique electrode to perform homogenization calculations) or from several n-phase volumes combined together (e.g., meshing a full cell from anode and cathode volumes). Module inputs are segmented stacked tif files. Meshes can be generated for the whole volume (i.e., a unique mesh), for groups of phases (e.g., a first mesh for the union of positive current collector and cathode solid material, a second mesh for the union of separator and electrolyte within both electrodes, and a third mesh for the union of negative current collector and anode solid material), and for each phase, with meshes having conforming interfaces. The above choice depends on the modelling method: a monolithic model would require a single mesh for the whole volume, while a segregated model [8] – that solves domain sequentially – would need meshes per phase or per group of phases. The latter would use the conforming interfaces

to transfer information between meshes. Furthermore, two meshing generation approaches are available: (i) structured mesh with cuboid representation (simple, fast, and robust generation with high mesh quality cells, but requires a large number of vertices, has no surface smoothing and no mesh density control), and (ii) unstructured mesh (with mesh density control and produces smooth surface, but has variable mesh quality cell, may fail for large volume and/or volume with large number of phases and is computationally expensive to generate). The structured mesh is using a simple in-house algorithm while the unstructured mesh lies on Iso2mesh [18] with in-house mesh corrections added. Iso2mesh is using constrained Delaunay tetrahedralization (CGAL) for surface mesh extraction, Laplacian, Laplacian-HC, and low-pass filters for surface mesh smoothing, and Tetgen for volumetric mesh generation and adaptive mesh resolution. The module contains mesh quality calculation, mesh visualizations, and mesh export/conversions (.mat, .csv, .msh, .inp, .stl) using Iso2mesh built-in functions. The .mat and .csv files contain vertices coordinates, cell connectivities, and cell phase labels required to re-build from scratch meshes in a FEM software, as did with FEniCS [34] in a previous work [8], while the other file extensions can be used to import directly the as-generated meshes in software that support them (e.g. Abaqus).

In addition to the meshing operation, the module provides useful pre-processing steps: scaling (to accommodate electrodes volumes obtained with different image resolution), auto-cropping (to accommodate electrodes volumes with incompatible in-plane dimensions), and various morphology opening steps to ease the meshing generation. Morphology opening includes standard erosion-dilatation, but also in-house algorithms to correct voxel-voxel connections (line-line and vertice-vertice connectivity are detected and removed) that may otherwise create meshes with tetrahedron cells connected through a single vertex, thus inducing singular flux in FEM models likely to trigger numerical divergence.

### 3. Illustrative examples

Figs. 5–8 provides examples of the GUI, from various modules. Emphasis lies on user-friendliness with a step-by-step guided approach. Images have been taken as it is from the toolbox documentation with bullets and text inserts added to help users. At the exception of the meshing, results were obtained with a 16Gb RAM Windows laptop, for volumes in the range of 10 to 100 million voxels.

Figs. 8–11 provide selected results from various modules. Microstructure numerical generation (including additives) valuable to investigate ‘what if’ architectures and perform sensitivity analysis on microstructure geometries (cf. Fig. 8). Microstructure parameter segmentation-induced errors valuable to track error propagations from segmentation uncertainty to microstructure parameters and eventually to electrochemical performances (cf. Fig. 9). Particle identification and size/morphology analysis using a discrete particle size algorithm to provide accurate average particle diameter for macroscale models and a simplified equivalent graph representation of the active material (cf. Fig. 10, top row). Representative volume element analysis performed on volume fraction relevant to determine if volume analysed is large enough to be representative, thus indicating the level of confidence of the microstructure analysis (cf. Fig. 10, bottom row). Microstructure mesh used for Finite Element Method calculations (cf. Fig. 11). Workstation with 64 GB RAM has been used to generate unstructured meshes with up to 50 million vertices using tortuous X-ray computed tomography 3D volumes of LIB electrodes.

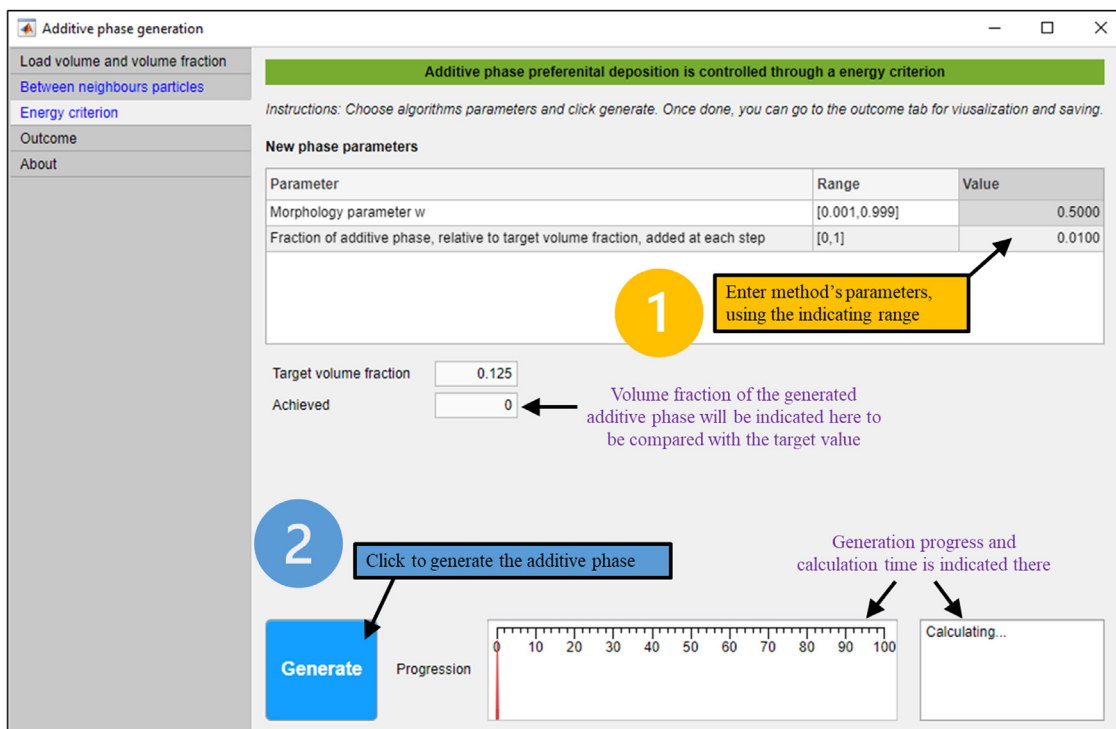


Fig. 5. (Generation module.) GUI for additive generation submodule using energy criterion method. GUI is organized in tabs to guide the user.

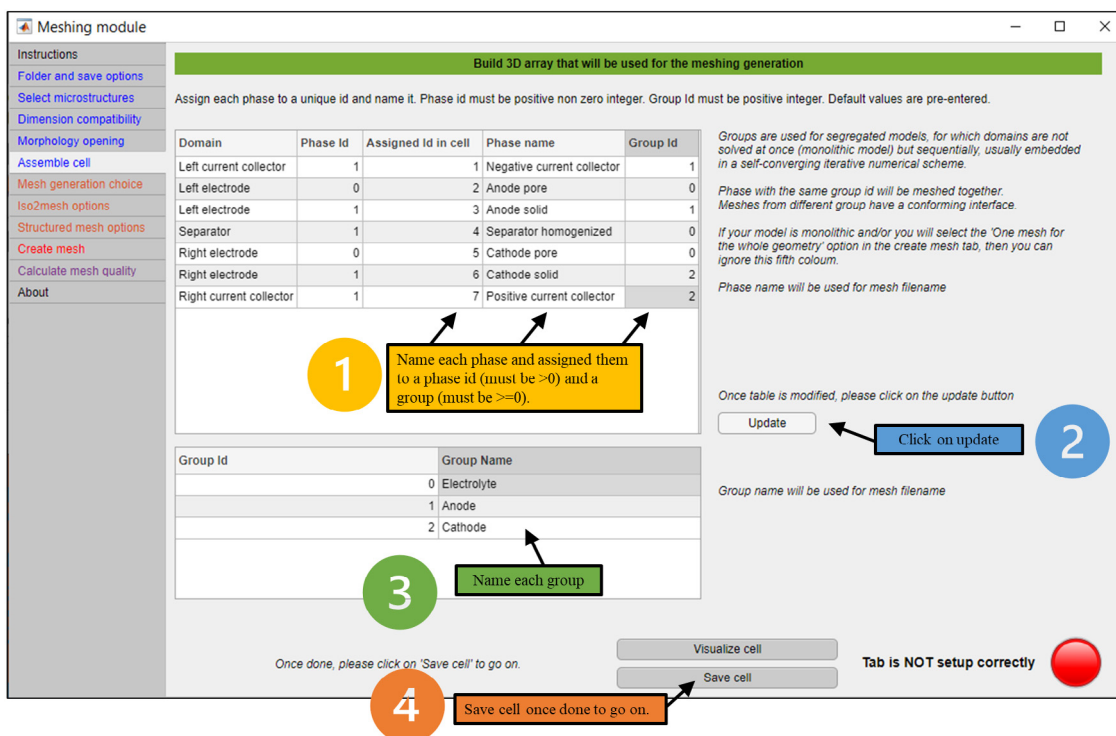


Fig. 6. (Meshing module.) GUI for cell meshing. Full cell case with each material assigned to a phase and a group for use in a segregated model.

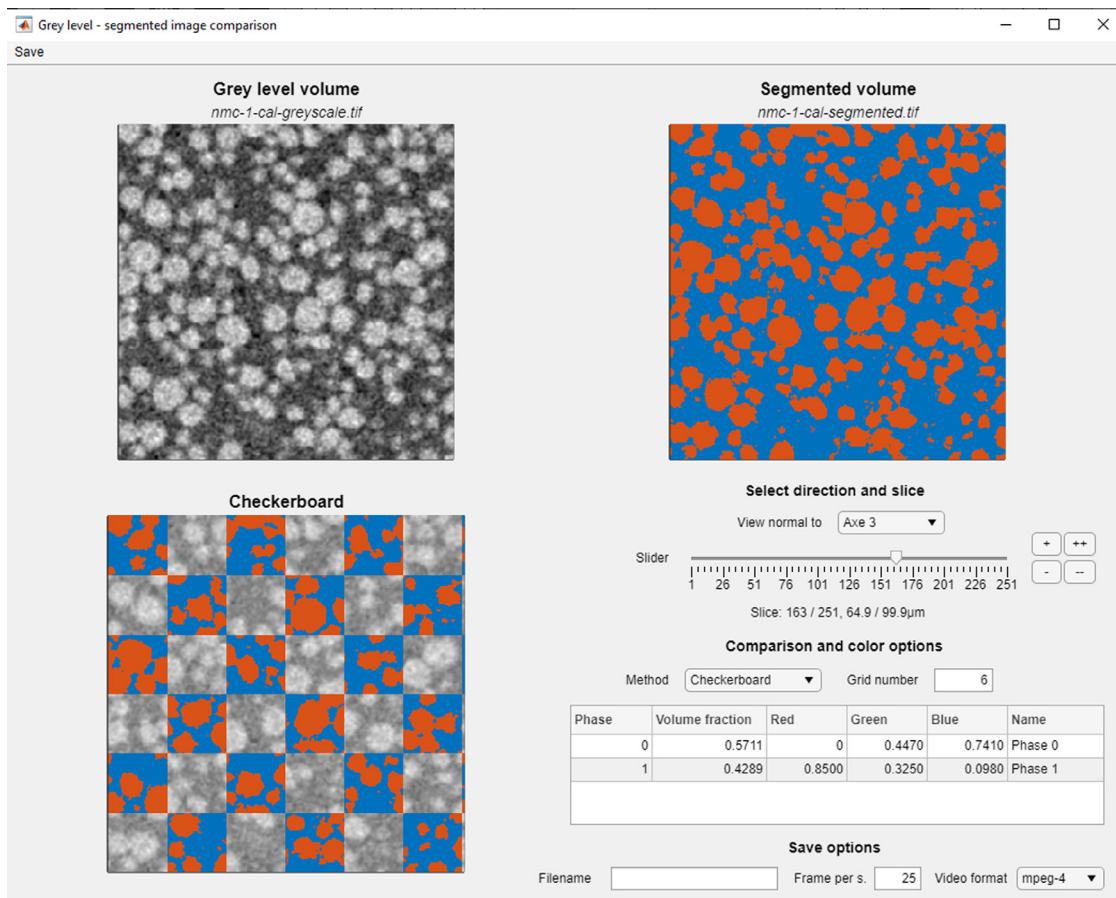


Fig. 7. (Visualization module.) GUI for grey level/segmented volumes comparison submodule. User can choose between an overlay (not shown) and a checkerboard (shown) comparison.

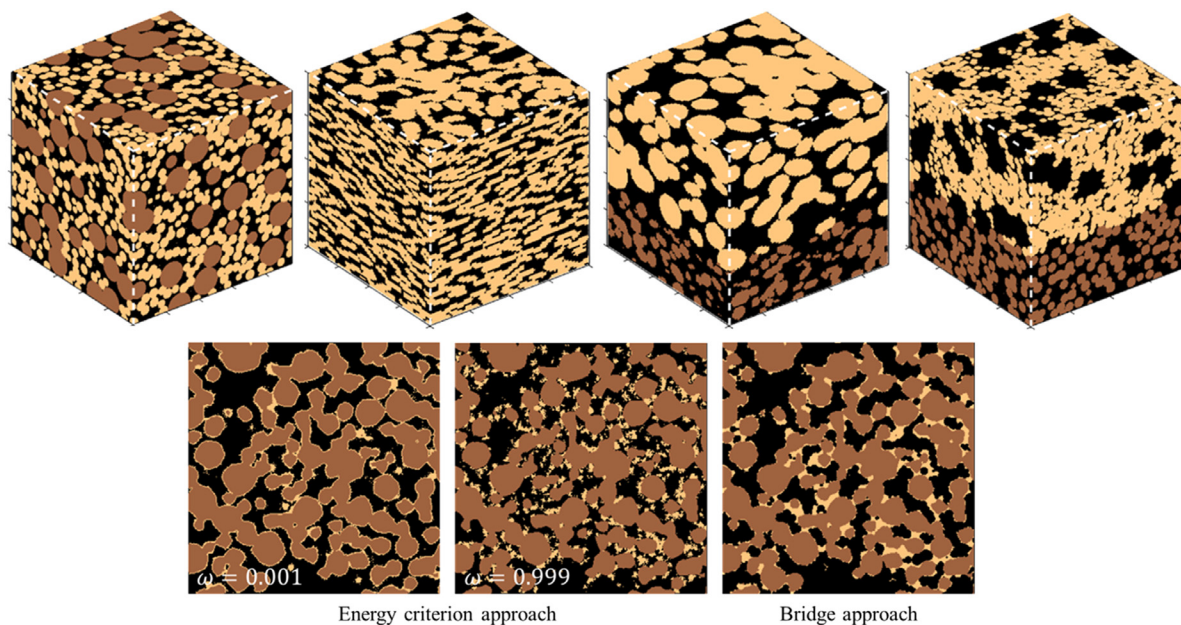
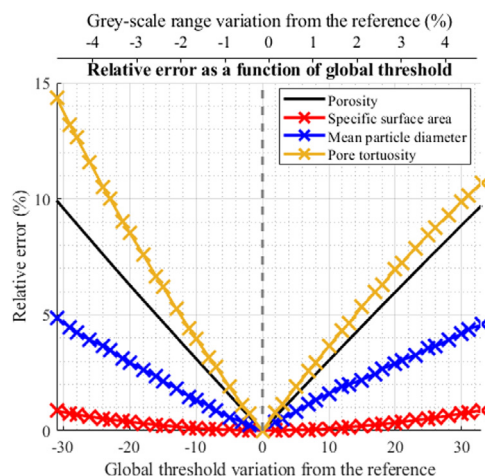


Fig. 8. (Generation module.) Example of microstructure generation. (Top, from left to right) bi-modal size distribution, ellipsoids with a preferential orientation, bi-layer with different porosity, particle size, particle alignment and orientation between the two layers, and bi-layer with pore former. (Bottom, from left to right) Additive phase added to an existing microstructure, using energetic approach with two extremes values, and using the bridge approach. Images have been produced using the visualization module once microstructure generations completed.



**Fig. 9.** (Segmentation module.) Relative error on microstructure parameters induced by an uncertainty on the segmentation between two user-defined threshold bounds. Because grey-level unit variation is subjective to the image format (e.g., 8 bits or 16 bits), the grey-level variation is also expressed in percentage of the min–max grey level range. In this example the tortuosity factor has the highest segmentation-induced error.

#### 4. Impact

MATBOX is expected to keep growing with new algorithms, both in-house and from third parties, with the goal to set a reference in the field of electrode microstructure analysis. The toolbox has dramatically streamlined otherwise time-consuming tasks such as microstructure characterization and enable wide design space analysis, respectively to provide microstructure parameters for macroscale LIB modelling and to identify promising electrode architectures for LIB fast charging [35]. Furthermore, the automated history log of the segmentation module significantly helps to keep records of the different steps involved in the segmentation process, which has improved segmentation reproducibility and enabled a systematic approach (i.e., coherent between samples) for the segmentation of dozens of microstructures. The GUI proved to be very time-efficient for intermittent microstructure analysis and for newcomers as its learning curve is much faster than using a standard code. Documentation provides detailed instructions on how to implement new algorithms in the characterization module GUI for user-made in-depth customization of the module for specific application.

While other (commercial or not) software delivers similar features, MATBOX offers a selection of algorithms and methods tailored for, but not restricted to, LIB modelling. For instance, RVE analysis offers control of the subvolume aspect ratio, therefore enabling determining the representative *section area* of an electrode (essential to evaluate the level of confidence of the characterization analysis), using subvolumes with thicknesses set equal to the electrode thickness as the latter is a characteristic of the electrode that will drive the concentration gradients. Microstructure generation algorithms have been developed to generate architectures relevant for LIB application (e.g., highly dense electrodes, graded electrodes, and aligned particles), especially for fast charge application [35]. Lastly, the meshing module can load 5 different volumes (two current collectors, two electrodes, and one separator) and combine them to produce a LIB full cell mesh ready to use, while requiring for inputs only 3D stack tiff files which are the usual format from X-ray Computed Tomography used in the LIB field, for a more efficient workflow.

Currently MATBOX is mainly used in the NREL energy storage group for LIB modelling, specifically for microstructure characterization [1,15,16], meshing [8], and numerical generation for

design space analysis [35]. However, MATBOX is being utilized by other groups within and outside NREL in fields not restricted to LIB. Researchers in the Advanced Power Electronics and Electric Machines (APEEM) Group at NREL have used MATBOX to model the porosity structure within sintered silver joints for thermal and thermomechanical evaluations. This porosity amount can change when the synthesis parameters of temperature and pressure are varied for die- and substrate-attach sintered silver layers within power electronics modules. Creating this structure would be very difficult in a traditional CAD program so APEEM researchers have leveraged the capabilities of this MATLAB toolbox. NREL researchers in the Renewable Resources and Enabling Sciences Center are using MATBOX for an upcoming publication comparing the differences in porosity and pore structure of wood and biochar to increase the accuracy of modelling the renewable energy production technology known as pyrolysis. Xuekun Lu from University College London has used MATBOX to investigate the effect of particle orientation on the electrode performance, as well as the advantage of hierarchical microstructures in improving the battery rate performance. A manuscript related to these are under preparation. Prehit Patel and George Nelson from the University of Alabama in Huntsville have been using MATBOX for the analysis of X-ray CT data for low cobalt LIB cathodes. In addition, MATBOX has been presented to other research institutions and industries with on-going discussion to implement new algorithms.

#### 5. Conclusions

The application, MATBOX, presented in this article allows for a highly automated microstructure characterization, in addition to providing relevant algorithms and methods for microstructure segmentation, meshing, and generation. The toolbox is divided into submodules with an emphasis on user-friendliness thanks to GUIs to improve productivity and reduce the learning curve. This makes the toolbox an easy-to-use all-in-one solution for microstructure numerical analysis. It is hoped the toolbox will keep growing eventually providing the LIB community with a standardized tool for microstructure/heterogeneous materials analysis.

#### Declaration of competing interest

The authors declare that they have no known competing financial interests or personal relationships that could have appeared to influence the work reported in this paper.

#### Acknowledgements

This software was authored by the National Renewable Energy Laboratory, operated by Alliance for Sustainable Energy, LLC, for the U.S. Department of Energy (DOE) under Contract No. DE-AC36-08G028308. Funding for algorithm development was provided by the U.S. DOE Vehicle Technologies Office's Computer-Aided Engineering of Batteries (CAEBAT) program [36] (program manager Brian Cunningham). Application of the algorithm for fast-charge analysis was provided by the eXtreme Fast Charge Cell Evaluation of Lithium-Ion Batteries (XCEL) program (program manager Samuel Gillard). I would like to thank my NREL colleagues, Dr. Donal Finegan and Dr. Andrew Colclasure for interesting discussions and suggestions about microstructure analysis. A.M. gratefully acknowledges support from Argonne National Laboratory. Argonne National Laboratory is operated for the U.S. Department of Energy Office of Science by UChicago Argonne, LLC, under contract number DE-AC02-06CH11357.



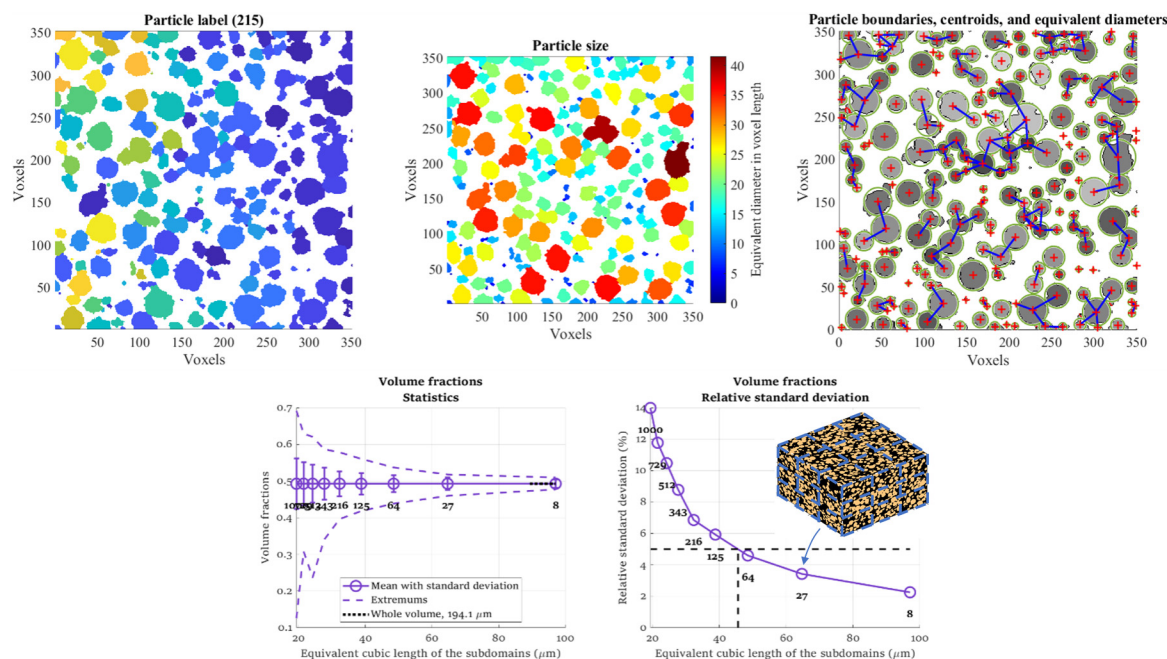


**Fig. 10.** (Characterization module.) (Top, from left to right) Particle identification (each particle, 215 in total, is assigned to a unique label/colour), equivalent particle diameter, and graph representation calculated with a d-PSD algorithm on a 2D slice (algorithm works in 3D). (Bottom) Example of a RVE analysis performed on volume fraction (left: extremes, standard deviation and average, right: standard deviation, both as function of subdomain size). Numbers (8, 27, 64, etc.) indicate the number of subvolumes. Insert shows FOV divided into subvolumes with the same aspect ratio of the whole volume (aspect ratio is customizable – see documentation of example). Volume fraction RVE size is  $\sim 45 \times 45 \times 45 \mu\text{m}^3$  in this example, using a 5% relative standard deviation threshold.

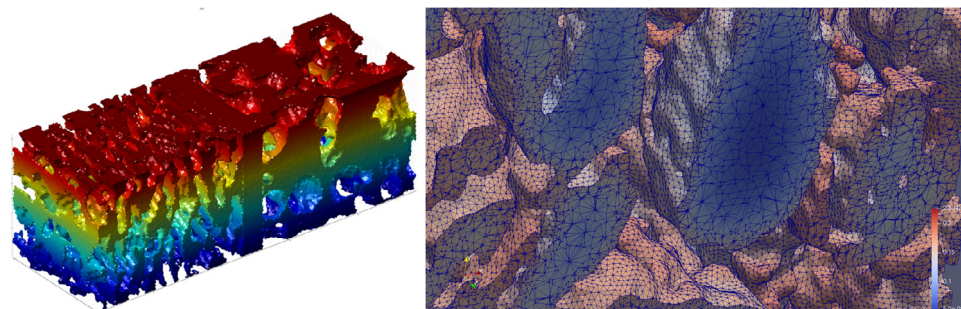


**Fig. 11.** (Meshing module.) (Left) electrolyte unstructured mesh, union of electrolyte domains of both electrodes and the separator. Colour is z-axis. (Right) Zoom on the solid concentration calculated with a LIB microscale electrochemical model [8] using a mesh provided by this module, revealing complex geometry and smooth surface.

## References

- [1] Usseglio-Viretta FL, Colclasure A, Mistry AN, Claver K, Pouraghajan F, et al. Resolving the discrepancy in tortuosity factor estimation for li-ion battery electrodes through micro-macro modeling and experiment. *J Electrochem Soc* 2018;165:A3403–26. <http://dx.doi.org/10.1149/2.0731814jes>.
- [2] Colclasure AM, Tanim TR, Jansen AN, Trask SE, Dunlop AR, et al. Electrode scale and electrolyte transport effects on extreme fast charging of lithium-ion cells. *Electrochim Acta* 2020;337:135854. <http://dx.doi.org/10.1016/j.electacta.2020.135854>.
- [3] Smith K, Wang C-Y. Power and thermal characterization of a lithium-ion battery pack for hybrid-electric vehicles. *J Power Sources* 2006;160. <http://dx.doi.org/10.1016/j.jpowsour.2006.01.038>.
- [4] Doyle M. Modeling of galvanostatic charge and discharge of the lithium/polymer/insertion cell. *J Electrochem Soc* 1993;140:1526. <http://dx.doi.org/10.1149/1.2221597>.
- [5] Pietsch P, Wood V. X-ray tomography for lithium ion battery research: a practical guide. *Annu Rev Mater Res* 2016;47:1–29. <http://dx.doi.org/10.1146/annurev-matsci-070616-123957>.
- [6] Eastwood DS, Bradley RS, Tariq F, Cooper SJ, Taiwo OO, et al. The application of phase contrast X-ray techniques for imaging Li-ion battery electrodes. *Nucl Instrum Methods Phys Res Section B Beam Interact Mater Atoms* 2014;324:118–23. <http://dx.doi.org/10.1016/j.nimb.2013.08.066>.
- [7] Colclasure AM, Dunlop AR, Trask SE, Polzin BJ, Jansen AN, et al. Requirements for enabling extreme fast charging of high energy density li-ion cells while avoiding lithium plating. *J Electrochem Soc* 2019;166:A1412–24. <http://dx.doi.org/10.1149/2.0451908jes>.
- [8] Allen JM, Chang J, Usseglio-Viretta FLE, Graf P, Smith K. A segregated approach for modeling the electrochemistry in the 3-d microstructure of li-ion batteries and its acceleration using block preconditioners. *J Sci Comput* 2021;86:42. <http://dx.doi.org/10.1007/s10915-021-01410-5>.
- [9] Higa K, Wu S-L, Parkinson DY, Fu Y, Ferreira S, et al. Comparing macroscale and microscale simulations of porous battery electrodes. *J Electrochem Soc* 2017;164:E3473–88. <http://dx.doi.org/10.1149/2.0501711jes>.
- [10] Danner T, Singh M, Hein S, Kaiser J, Hahn H, et al. Thick electrodes for li-ion batteries: a model based analysis, Vol. 334. 2016. <http://dx.doi.org/10.1016/j.jpowsour.2016.09.143>.
- [11] Hutzenlaub T, Thiele S, Paust N, Spotnitz R, Zengerle R, et al. Three-dimensional electrochemical li-ion battery modelling featuring a focused ion-beam/scanning electron microscopy based three-phase reconstruction of a LiCoO<sub>2</sub> cathode. *Electrochim Acta* 2014;115. <http://dx.doi.org/10.1016/j.electacta.2013.10.103>.
- [12] Roberts SA, Mendoza H, Brunini VE, Trembacki BL, Noble DR, et al. Insights into lithium-ion battery degradation and safety mechanisms from mesoscale simulations using experimentally-reconstructed mesostructures. *J Electrochem Energy Convers Storage* 2016. <http://dx.doi.org/10.1115/1.4034410>.
- [13] Lu X, Bertel A, Finegan DP, Tan C, Daemi SR, et al. 3D microstructure design of lithium-ion battery electrodes assisted by X-ray nano-computed

- tomography and modelling. *Nature Commun* 2020;11:2079. <http://dx.doi.org/10.1038/s41467-020-15811-x>.
- [14] Xu R, Yang Y, Yin F, Liu P, Cloetens P, et al. Heterogeneous damage in lithium batteries: Experimental analysis and theoretical modeling. *J Mech Phys Solids* 2019;129:160–83. <http://dx.doi.org/10.1016/j.jmps.2019.05.003>.
- [15] Usseglio-Viretta F, Smith K. Quantitative microstructure characterization of a NMC electrode. *ECS Trans* 2017;77:1095–118. <http://dx.doi.org/10.1149/07711.1095ecst>.
- [16] USSEGLIO-VIRETTA FLE, Finegan D, Colclasure AM, Heenan T, Abraham DP, et al. Quantitative relationships between pore tortuosity, pore topology, and solid particle morphology using a novel discrete particle size algorithm. *J Electrochem Soc* 2020. <http://dx.doi.org/10.1149/1945-7111/ab913b>.
- [17] Cooper SJ, Bertei A, Shearing PR, Kilner JA, Brandon NP. TauFactor: An open-source application for calculating tortuosity factors from tomographic data. *SoftwareX* 2016;5:203–10. <http://dx.doi.org/10.1016/j.softx.2016.09.002>.
- [18] Fang Q, Boas DA. Tetrahedral mesh generation from volumetric binary and grayscale images. In: 2009 IEEE Int Symposium Biomed Imaging Nano Macro. 2009, p. 1142–5. <http://dx.doi.org/10.1109/isbi.2009.5193259>.
- [19] Crosby K. Column converter for excel, MATLAB central file exchange, column converter for excel, MATLAB central file exchange. 2020. <https://www.mathworks.com/matlabcentral/fileexchange/28343-column-converter-for-excel> (accessed 2020).
- [20] Jan, DataHash. Matlab central file exchange, DataHash, MATLAB central file exchange. (n.d.). 2020. <https://www.mathworks.com/matlabcentral/fileexchange/31272-datahash> (accessed 2020).
- [21] Tanaka M. Noise level estimation from a single image, MATLAB central file exchange, noise level estimation from a single image, MATLAB central file exchange. 2020. <https://www.mathworks.com/matlabcentral/fileexchange/36921-noise-level-estimation-from-a-single-image> (accessed 2020).
- [22] Altman Y. ScreenCapture - get a screen-capture of a figure frame or component. In: Screenshot - get a screen-capture of a figure frame or component. 2021. <https://www.mathworks.com/matlabcentral/fileexchange/24323-screenshot-get-a-screen-capture-of-a-figure-frame-or-component> (accessed 2021).
- [23] Mistry A, Smith K, Mukherjee PP. Secondary phase stochastics in lithium-ion battery electrodes. *ACS Appl Mater Interf* 2018. <http://dx.doi.org/10.1021/acsami.7b17771>.
- [24] Mistry AN, Smith K, Mukherjee PP. Electrochemistry coupled mesoscale complexations in electrodes lead to thermo-electrochemical extremes. *ACS Appl Mater Interf* 2018;10:28644–55. <http://dx.doi.org/10.1021/acsami.8b08993>.
- [25] Song C, Wang P, Makse HA. A phase diagram for jammed matter. *Nature* 2008;453:629–32. <http://dx.doi.org/10.1038/nature06981>.
- [26] Trembacki BL, Mistry AN, Noble DR, Ferraro ME, Mukherjee PP, et al. Editors' choice—Mesoscale analysis of conductive binder domain morphology in lithium-ion battery electrodes. *J Electrochem Soc* 2018;165:E725–36. <http://dx.doi.org/10.1149/2.0981813jes>.
- [27] Trembacki BL, Noble DR, Brunini VE, Ferraro ME, Roberts SA. Mesoscale effective property simulations incorporating conductive binder. *J Electrochem Soc* 2017;164:E3613–26. <http://dx.doi.org/10.1149/2.0601711>.
- [28] Holzer L, Iwanschitz B, Hocker T, Münch B, Prestat M, et al. Microstructure degradation of cermet anodes for solid oxide fuel cells: Quantification of nickel grain growth in dry and in humid atmospheres. *J Power Sources* 2011;196. <http://dx.doi.org/10.1016/j.jpowsour.2010.08.017>.
- [29] Perona P, Malik J. Scale-space and edge detection using anisotropic diffusion. Vol. 12. 1990. <http://dx.doi.org/10.1109/34.56205>.
- [30] Buades A, Coll B, Morel J-M. A non-local algorithm for image denoising. In: IEEE computer society conference on computer vision and pattern recognition. CVPR'05, 2005. <http://dx.doi.org/10.1109/cvpr.2005.38>.
- [31] Otsu N. A threshold selection method from gray-level histograms, Vol. 9. 1979. <http://dx.doi.org/10.1109/tsmc.1979.4310076>.
- [32] NREL battery Microstructures Library. (2020). <https://www.nrel.gov/transportation/microstructure.html> (accessed May 15, 2020).
- [33] Kanit T, Forest S, Galliet I, Mounoury V, Jeulin D. Determination of the size of the representative volume element for random composites: statistical and numerical approach, Vol. 40. 2003. [http://dx.doi.org/10.1016/S0020-7683\(03\)00143-4](http://dx.doi.org/10.1016/S0020-7683(03)00143-4).
- [34] Alnaes MS, Blechta J, Hake J, Johansson A, Kehlet B, et al. The FEniCS project version 1.5. *Arch Numer Softw* 2015;3.
- [35] ANL, INL, NREL, SLAC, LBNL, et al. Extreme fast charge cell evaluation of lithium-ion batteries. 2019. <https://blogs.anl.gov/access/wp-content/uploads/sites/53/2019/09/Q3FY19-XCEL-Report.pdf>.
- [36] NREL's Computer-Aided Engineering for Electric Drive Vehicle Batteries (CAEBAT). NREL's computer-aided engineering for electric drive vehicle batteries (CAEBAT). (n.d.). <https://www.nrel.gov/transportation/caebat-microstructure-applications.html>.